Molecular, Thermal, and Morphological Characterization of Narrowly Branched Fractions of 1-Octene Linear Low-Density Polyethylene. 3. Lamellar and Spherulitic Morphology

F. Defoor, G. Groeninckx, and H. Reynaers*

Laboratorium voor Macromoleculaire Structuurchemie, Departement Scheikunde, Katholieke Universiteit Leuven, Celestijnenlaan 200F, B3001 Heverlee, Belgium

P. Schouterden and B. Van der Heijden

DOW BENELUX N.V., P.O. Box 48, 4530 AA Terneuzen, The Netherlands

Received September 1, 1992; Revised Manuscript Received December 21, 1992

ABSTRACT: The semicrystalline lamellar morphology, the crystalline phase, and the spherulitic structure of 1-octene linear low-density polyethylene (LLDPE) fractions with a narrow short chain branching distribution were studied. The average short chain branching content of the fractions studied increases from 2.9 to 28.2 branches per 1000 carbon atoms while the weight-average molecular weight concomitantly decreases from 2.7×10^5 to 1.9×10^4. Characteristic morphological parameters include the number-average lamellar thickness, the thickness of the crystalline core and of the transition layers, the periodicity of the lamellar stacks, the unit cell dimensions of the crystalline phase, and the average radius of the spherulites. The core thickness of the crystalline lamellae decreases and the transition layer thickness increases with increasing branching content. Fair agreement was found between the values of the lamellar thickness obtained in this study and those obtained in a previous TEM study. The expansion of the unit cell of the crystals with increasing branching content is related to a decrease of the thickness of the lamellae. The average spherulitic radius of the fractions decreases with increasing short chain branching content. The spherulitic morphology is deteriorated at high values of either the branching content or the molecular weight.

Introduction

Linear low-density polyethylenes (LLDPEs) are copolymers of ethylene and an α-olefin. The comonomer is incorporated as short side chain branches that affect the chain microstructure, the crystallization behavior, and the ultimate morphology of the copolymer. Commercial LLDPE samples normally have a heterogeneous chain microstructure characterized by a broad intermolecular distribution of the branching content and the molar mass. The crystallization and melting behavior of such samples is complex as evidenced by multiple melting endotherms during DSC analysis. From previous work it became clear that commercial LLDPEs should be considered as a complex blend with respect to both the chain microstructure and the molar mass.[1,2] The crystallization and melting process of such complex samples can only be understood by the evaluation of correlations between chain microstructure, crystallization kinetics, lamellar morphology, and crystal structure under carefully controlled experimental conditions. Consequently, there is a need for more homogeneous samples (fractions) of the copolymer to systematically investigate the influence of the branching content on the morphology as a whole.

Recently, a heterogeneous ethylene/1-octene copolymer (LLDPE A) was fractionated with respect to the short chain branching content. The fractionation method and the chain microstructure of the fractions have been reported elsewhere.[3] The fractions were shown to have a more homogeneous chain microstructure as compared to the original heterogeneous copolymer. The weight-average molecular weight of the fractions is inversely related to their short chain branching content. The branching content strongly influences the crystallization and melting behavior and the degree of crystallinity of the fractions. A quantitative TEM study of the lamellar morphology of the fractions and of the nonfractionated sample LLDPE A has been presented previously.[4] Thickness distributions of the crystalline lamellae and of the amorphous layers within the stacks have been determined. The average lamellar thickness decreases with increasing branching content. It has also been observed that the curvature and lateral dimensions of the lamellae are influenced by both the branching content and the molar mass. The observations are in agreement with earlier detailed studies by Voigt-Martin et al.[5,6]

In this paper (part 3) we describe the semicrystalline lamellar morphology, the crystallinity at the level of the unit cell, and the spherulitic morphology for the fractions of LLDPE A, as studied by scattering experiments. Small-angle X-ray scattering (SAXS) experiments provide detailed information on the thickness of the crystalline core and the transition layers of the lamellae through an evaluation of the scattering curves. The analysis of the scattering curves is presented and discussed in detail, and the physical parameters obtained are compared with the information obtained with TEM on the same samples. The crystalline phase is studied by wide-angle X-ray scattering (WAXS). Changes in the dimensions of the unit cell are related to the question whether the chain irregularities are incorporated into the crystalline lattice or completely segregated into the interlamellar amorphous regions. The results make clear that the structure of the crystalline lattice is related not only to the presence of the branches but also to a large extent to the thickness of the crystalline lamellae. Finally, lamellae can be arranged into different types of organization of higher order, commonly named as supermolecular structures. The spherulitic morphology is the most specific type of supermolecular organization, although it does not represent a universal mode of crystallization as shown by Mandelkern et al.[7] Lamellae can as well be organized into rodlike entities or be distributed randomly in an amorphous matrix. Detailed morphological maps relating the supermolecular organization with the chain microstructure

* To whom correspondence should be addressed.

0024-9297/93/2226-2575$04.00/0 © 1993 American Chemical Society

Table I. Short Chain Branching Content, Weight-Average Molecular Weight, and Polydispersity of the Fractions and LLDPE A

fraction	SCB (CH_3/1000 C)	$\bar{M}_w$	$\bar{M}_w/\bar{M}_n$
A1		19 100	3.98
A2	28.2	49 300	3.37
A3	20.4	94 000	2.86
A4	14.8	128 200	2.76
A5	11.5	146 200	2.75
A6	6.4	176 300	2.44
A7	3.2	252 000	2.20
A8	2.9	269 000	2.19
LLDPE A	9.7	114 000	3.67

and the crystallization conditions were presented by Mandelkern et al.,[8] Voigt-Martin et al.,[9] and Hosoda et al.[10] Small-angle laser light scattering (SALLS) experiments were used to characterize the superstructure, following Stein's description of the scattering patterns.[11-13]

Materials and Experimental Techniques

An ethylene/1-octene copolymer (LLDPE A) was used in this study. The average short chain branching content of sample LLDPE A measured 9.7 branches per 1000 carbon atoms; it has a weight-average molecular weight of 1.1×10^5 and a polydispersity of 3.67. From the heterogeneous LLDPE A sample, eight fractions (A1–A8) with a more homogeneous chain microstructure were obtained using a preparative temperature rising elution fractionation technique. Detailed information on the fractionation procedure and the chain microstructure was presented in part 1 of this series.[3] The average branching content of the fractions studied increases from 2.9 to 28.2 branches per 1000 carbon atoms, and the weight-average molecular weight concomitantly decreases from 2.7×10^5 to 1.9×10^4. The average short chain branching content, the weight-average molecular weight, and the polydispersity of the LLDPE A sample and the eight fractions are given in Table I. The samples were melted at 150 °C during 10 min and then crystallized at a cooling rate of 5 °C/min.

All SAXS measurements were performed at room temperature with a Rigaku type Kratky camera using infinite slit geometry. Ni-filtered Cu radiation was obtained from a Rigaku rotating-anode generator operating at 50 kV and 150 mA. Scattering patterns were recorded with a Braun position-sensitive detector. The distance between sample and detector was 30.5 cm. Scattering data were collected in the angular range between 0.01 and 5.0° 2θ using 650 channels of the detector.

Wide-angle X-ray diffractograms were obtained at room temperature using Ni-filtered Cu Kα radiation obtained from a Philips PW 1730 X-ray generator. A Debye–Scherrer camera (radius 57.3 mm and Straumanis arrangement) was used on account of the limited amount of material needed to acquire the WAXS spectra. A quantitative evaluation of the intensity in the angular range between 10 and 60° 2θ was feasible with a microdensitometer. The diffractograms were corrected for background scattering. The crystalline peaks were separated from the amorphous halo using a least-squares fitting program[14] assuming the diffraction peak profiles to be intermediate between Lorentzian and Gaussian. The 110, 200, 210, 020, 011, 310, 111, 201, and 220 reflections were used to calculate the unit cell parameters a and b using a least-squares cell-parameter program.[15]

Small-angle laser light scattering patterns were recorded using an in-house made SALLS apparatus including a He/Ne laser light source and a CCD camera as detector.[16] The H_v scattering patterns were stored and processed using an image analysis system. The samples (thin films of approximately 50 μm) were placed between cover glasses; they were held at 150 °C during 10 min and subsequently cooled at 5 °C/min.

Small-Angle X-ray Scattering (SAXS)

Introduction. The mean thickness of crystalline lamellae in a spherulitic superstructure has been generally estimated from an analysis of the experimental small-angle X-ray scattering curves, assuming a two-phase

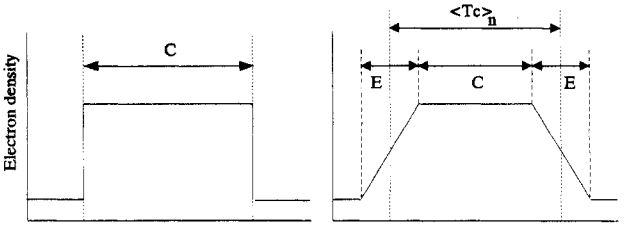

Figure 1. Electron density profile perpendicular to the lamellae for the two-phase model (left) and the pseudo-two-phase model (right).

structure. The semicrystalline morphology is then considered to consist of alternating crystalline and amorphous layers, which are parallel and separated by sharp phase boundaries. The electron density profile perpendicular to the lamellae of such a structure is shown in Figure 1 (left). The lamellar thickness C_l is then often calculated using the relation $C_l = \phi L$, where ϕ is the volume crystallinity of the sample (as obtained by other methods such as DSC or density measurements) and L is the one-dimensional periodicity, i.e., the sum of the average thicknesses of crystalline and amorphous layers.

The now generally accepted pseudo-two-phase model assumes that the crystalline lamellae consist of a crystalline core of thickness C and transition layers of thickness E. The electron density profile perpendicular to the lamellae, represented in Figure 1 (right), is characterized by a linear variation of the electron density with distance in the transition layer, on going from a crystalline to an amorphous layer. All relevant morphological parameters describing the pseudo-two-phase model, as given in Figure 1 (right), can be obtained from the experimental scattering data either by the correlation function approach or by the direct analysis. The correlation function method was originally proposed by Vonk and Kortleve[17] for an ideal two-phase system. A more elaborate analysis of the correlation function approach has been presented by Strobl et al.,[18,19] allowing for the evaluation of the full information content using a simple geometrical construction. A similar analysis, which is used in this work, has been presented by Vonk et al.[20] In the direct analysis method, which has been reviewed by Crist,[21] one compares the experimental scattering curve to a calculated scattering curve, based on the assumed physical model and the model parameters searched for. In the present work the transition layer thickness E has been obtained by the analysis of the scattering curve as shown by Vonk et al.[22] The crystalline core thickness C was calculated using the correlation function method of Vonk.[20,22] The use of the one-dimensional correlation function to calculate the average lamellar thickness is valid for any pseudo-two-phase structure with a transition layer having a linear density gradient.[22]

Processing of the SAXS Curves. The angular dependence of the small-angle X-ray scattering is usually expressed in terms of the scattering vector $s = (2/\lambda)\sin\theta$, where θ is half the scattering angle. The processing of the SAXS measurements in calculating the morphological parameters as shown in Figure 1 involves several steps. The blank scattering was subtracted from the sample scattering after correction for the sample thickness and absorption. The continuous background scattering I_b was accounted for by fitting the intensity in the angular range between 2 and 5° 2θ by the equation $I_b = a + bs^n$, where a and b are constants and n is an even number giving the best fit.[20] After subtraction of the background scattering I_b from the sample scattering, the smeared intensity $\tilde{I}(s)$

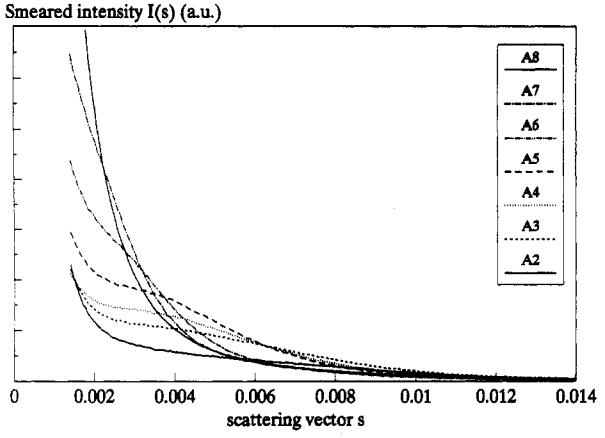

Figure 2. Smeared scattering curves $\tilde{I}(s)$ of the fractions as a function of the scattering vector s.

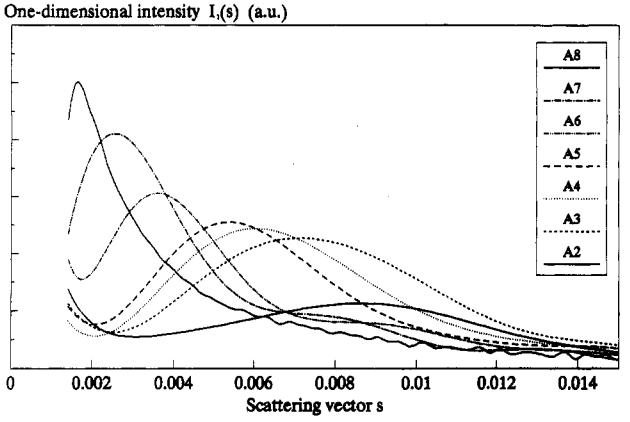

Figure 3. One-dimensional scattering function $I_1(s)$ of the fractions as a function of the scattering vector s.

Table II. Short Chain Branching Content, Periodicity L, Volume Crystallinity ϕ, and Lamellar Thickness C_l of the Fractions and LLDPE A

sample	SCB (CH_3/1000 C)	L (Å)	ϕ (%)	C_l (Å)
A2	28.2	116	21	24
A3	20.4	140	31	43
A4	14.8	166	31	51
A5	11.5	187	38	70
A6	6.4	275	47	130
A7	3.2	369	44	163
A8	2.9		50	
LLDPE A	9.7	191	34	64

is obtained. Subsequently, for the application of the two-phase model, the corresponding pinhole collimation scattering profile $I(s)$ is calculated by "desmearing" of $\tilde{I}(s)$. The one-dimensional scattering function $I_1(s)$, corresponding to the scattering profile of lamellar stacks perpendicular to the layers, is obtained from the desmeared scattering function $I(s)$ using the Lorentz correction, $I_1(s) = 4\pi s^2 I(s)$. The one-dimensional periodicity L can then be calculated by applying Bragg's law to the scattering maximum in the one-dimensional scattering function ($4\pi s^2 I(s)$ vs s). On the other hand, to obtain the crystalline core thickness C described in the pseudo-two-phase model, the one-dimensional correlation function $\gamma_1(x)$ is calculated directly from the smeared $\tilde{I}(s)$ data.[17] Processing of the small-angle X-ray scattering data (background correction, desmearing, and calculation of the correlation function) was done with the FFSAXS-5 program.[23]

The small-angle X-ray scattering curves were first analyzed according to the simple two-phase model. The smeared scattering curves $\tilde{I}(s)$ and the corresponding one-dimensional scattering intensity curves $I_1(s)$ of the fractions A2–A8 are plotted as a function of the scattering vector s in Figures 2 and 3, respectively.

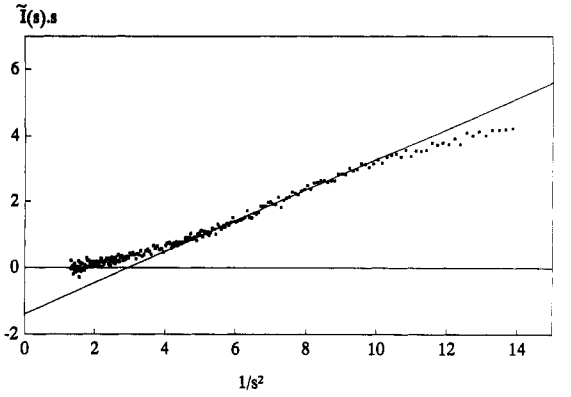

Figure 4. $\tilde{I}(s)s$ versus $1/s^2$ plot for fraction A2.

One observes a gradual shift of the maximum of the one-dimensional scattering function $I_1(s)$ toward lower angles as a function of decreasing branching content of the fractions. This observation points to an increase of the one-dimensional periodicity L, which can be attributed to an increase of the thickness of the crystalline and/or amorphous layers. However, for fractions A7 and A8, involving the lowest branching content and the highest molar mass, the smeared intensity function $\tilde{I}(s)$ exhibits a continuously decreasing scattering. It has been shown by Voigt-Martin et al. that such a scattering curve is indicative for the absence of regular lamellar stacks.[24] Consequently, the assumed ideal lamellar model is not a suitable description of the real lamellar morphology, which makes the interpretation of the increase of the periodicity L questionable. The lamellar thickness C_l calculated from the periodicity L and the volume crystallinity ϕ, assuming the ideal lamellar two-phase structure, is given in Table II. The volume crystallinity ϕ was calculated from the overall crystallinity χ_c measured with DSC (part 1), using relation 1. In this relation ρ_a and ρ_c are the amorphous and the crystalline density respectively.[25] The values of ρ_c are obtained from the WAXS experiments, while a value of 0.85 was used for ρ_a.[26]

$$\phi = 1/\left(1 + \frac{1-\chi_c}{\chi_c}\frac{\rho_c}{\rho_a}\right) \quad (1)$$

A more elaborate analysis of the experimental scattering data in terms of the pseudo-two-phase concept, as proposed by Vonk, is now discussed. The tail region of the smeared scattering intensity for samples exhibiting a pseudo-two-phase morphology can be approximated by

$$\tilde{I}(s) = (\pi c/2)(1/s^3 - 2\pi^2 E^2/3s) \quad (2)$$

where all the symbols have their usual significance and c is a constant.[20] As was shown by Vonk,[22] this relation can be used to determine the thickness E of the transition layer from an $\tilde{I}(s)s$ versus $1/s^2$ plot. A typical plot for fraction A2 is given in Figure 4. The slope of the straight part of the plot equals $\pi c/2$ and the intercept equals $-\pi^3 c E^2/3$. The standard deviation of the values calculated for the transition layer thickness E is about 2 Å, when the absolute value of the transition layer exceeds 10 Å. This was estimated by checking the influence of different reasonable fitting procedures for the background scattering intensity I_b and secondly by applying different fitting ranges in the $\tilde{I}(s)s$ versus $1/s^2$ plot.

When the thickness of the transition layer is lower than 10 Å, the intercept of the straight part comes very close

Table III. Short Chain Branching Content, Number-Average Lamellar Thickness $\langle T_c \rangle_n$, Transition Layer Thickness E, and Core Thickness C of the Fractions and LLDPE A

sample	SCB (CH_3/1000 C)	$\langle T_c \rangle_n$ (Å)	E (Å)	C (Å)
A2	28.2	38	21	18
A3	20.4	44	21	22
A4	14.8	47	18	29
A5	11.5	57	16	41
A6	6.4	78	15	64
A7	3.2	88	7	81
A8	2.9	105	8	97
LLDPE A	9.7	50	16	34

to the origin, which makes the calculated values of the transition layer less reliable. The thickness of the transition layers E of the different fractions and the nonfractionated LLDPE A are given in Table III. The transition layer thickness E increases from about 7 to 21 Å with increasing short chain branching content; these values are reasonable compared to the results obtained for other ethylene copolymer samples by Vonk[22] using SAXS and by Alamo et al.[27] using the Raman internal modes technique. The transition layer E becomes thicker with increasing short chain branching content since most of the chain irregularities are rejected from the crystalline core. The crowding of these noncrystallizable bulky units at the surface induces consequently a packing problem of the molecular chains.[5,27]

The influence of the molecular weight—known as the entanglement effect—on the morphological properties studied is significant, as has been shown frequently in the literature.[27-32] For the fractions studied, the molecular weight and the short chain branching content cannot be treated as independent variables, since they are inversely related. The increase of the transition layer thickness therefore needs to be evaluated carefully.

It was shown by Mandelkern et al.[29] that for linear polyethylene fractions an increased molecular weight results in a thickening of the transition layer. Also, it was revealed by Alamo et al.[33] that a preferential accumulation of the branches in the interphase of the copolymeric crystal overcomes the entanglement effect; copolymers having a fixed branching content exhibit an invariance of the interfacial content with increasing molecular weight. Consequently, since for the fractions studied, the molecular weight even decreases as the branching content increases, the increase of the transition layer thickness must be recognized as an effect of the short-chain branches. Furthermore, our conclusions are sustained by additional information on the effect of the molecular weight obtained in a parallel study on fractions from two other ethylene/1-octene copolymer samples—LLDPE B and LLDPE C—having identical branching contents but different molecular weights.[34] In the pseudo-two-phase model the number-average thickness $\langle T_c \rangle_n$ of the crystalline lamellae is defined as the distance enclosed by the midplanes of the transition layers (Figure 1) and can be determined from the one-dimensional correlation function $\gamma_1(x)$.

$$\gamma_1(x) = \frac{\int_0^\infty \tilde{I}(s) s [J_0(z) - z J_1(z)]\, ds}{\int_0^\infty \tilde{I}(s) s\, ds} \qquad (3)$$

where J_0 and J_1 are the first- and second-order Bessel functions.

A typical one-dimensional correlation function (sample A2) is given in Figure 5. The horizontal baseline in Figure 5 was constructed at $-\phi/(1-\phi)$, where ϕ is the volume crystallinity estimated from the overall crystallinity[18,22]

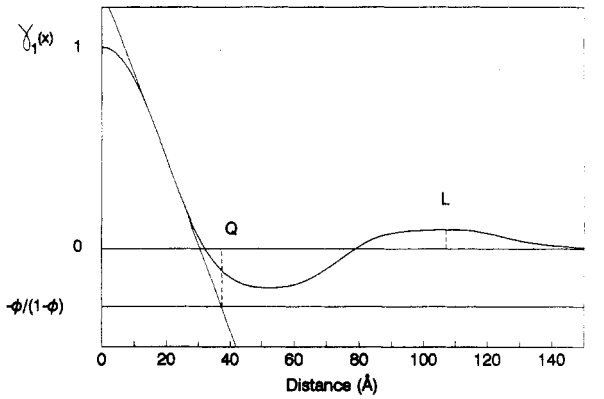

Figure 5. One-dimensional correlation function of fraction A2.

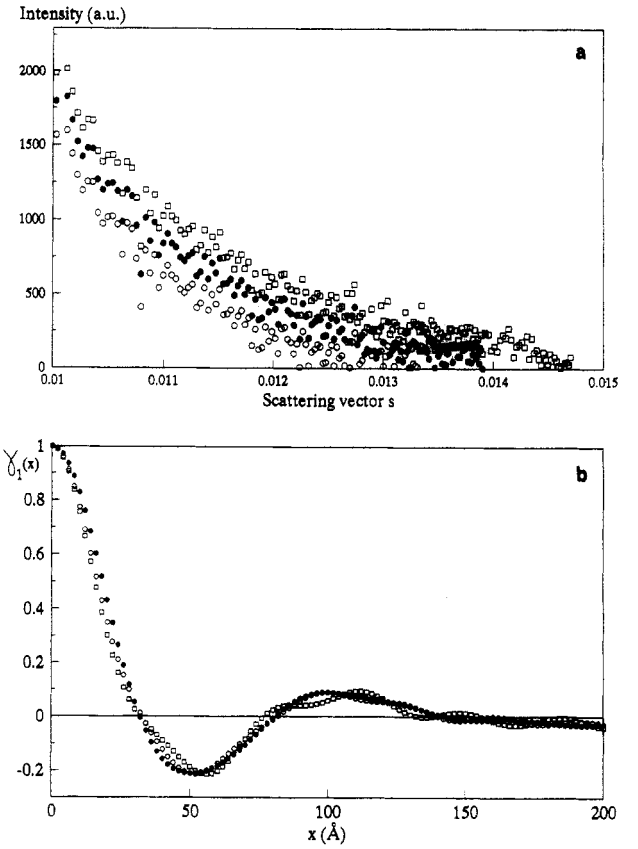

Figure 6. (a) Scattering intensity $\tilde{I}(s)$ obtained after subtraction of three different corrections and (b) the corresponding correlation functions.

with relation 1. Subsequently, $\langle T_c \rangle_n$ is given by the intersection OQ of the baseline with the tangent of the self-correlation part of $\gamma_1(x)$. This intercept has to be corrected by a factor depending on the transition layer thickness E and the volume crystallinity ϕ according to[22]

$$\langle T_c \rangle_n = \mathrm{OQ} + \frac{E}{3} \frac{\phi}{1-\phi} \qquad (4)$$

The accuracy of the values obtained for $\langle T_c \rangle_n$ consequently depends on the shape of the one-dimensional correlation function $\gamma_1(x)$ in the self-correlation part and on the correctness of the values used for the volume crystallinity ϕ and the transition layer thickness E. The effect of the background correction on the shape of the correlation function is illustrated in Figure 6. Three different background corrections and the corresponding correlation functions are plotted in parts a and b of Figure 6, respectively. The one-dimensional correlation function $\gamma_1(x)$ clearly suffers from a high-frequency modulation when the background is not accounted for properly.

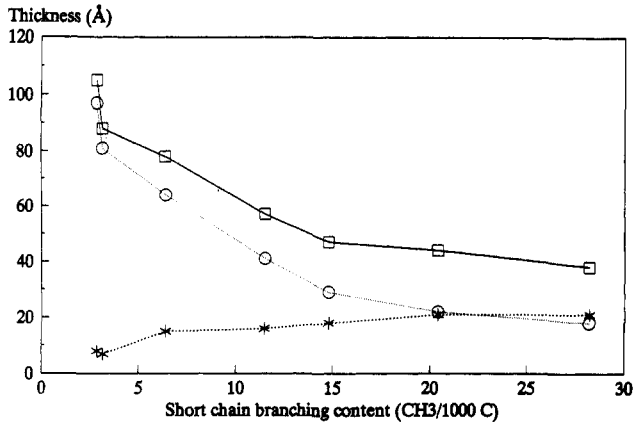

Figure 7. Number-average lamellar thickness $\langle T_c \rangle_n$ (□), core thickness C (○), and transition layer thickness E (*) as a function of the short chain branching content.

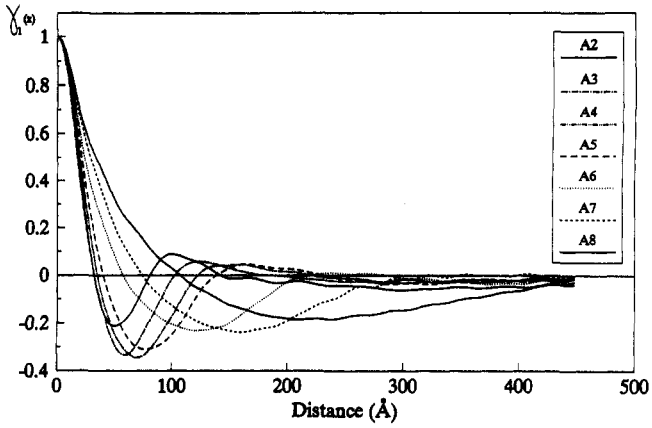

Figure 8. One-dimensional correlation function of the fractions.

Nevertheless, the overall shape of the correlation function remains nearly unchanged.

Secondly, the effect of the baseline position on the values calculated for $\langle T_c \rangle_n$ has been probed by varying the volume crystallinity by 10%. The standard deviation obtained for $\langle T_c \rangle_n$ due to the variation of the background correction and the variation of the volume crystallinity has been estimated to be 3 Å. The uncertainty with respect to the values used for the transition layer thickness is not included in the estimation of this standard deviation; the true standard deviation is hence presumed to be higher.

Subsequently, the values calculated for the number-average lamellar thickness $\langle T_c \rangle_n$ can be combined with the transition layer thickness E, to estimate the thickness C of the lamellar core: $C = \langle T_c \rangle_n - E$. The results for the core thickness C, the transition layer thickness E, and the number-average lamellar thickness $\langle T_c \rangle_n$ for all the samples are presented in Table III and plotted as a function of the short chain branching content in Figure 7. As the short chain branching content increases from 2.9 to 28.2 branches per 1000 C atoms, the core thickness C of the lamellae decreases from 97 to 18 Å while the transition layer thickness E increases from 8 to 21 Å. At the highest branching contents (fractions A2 and A3), the crystalline core of the lamellae becomes very thin and is of the same order of magnitude as the transition layers. The lowest value of the thickness of the crystalline core C was obtained for fraction A2 and measures about 18 Å. This value seems to be in reasonable agreement with the statement of Randall et al.[35] that a molecular chain must have a length of at least 6–10 ethylene sequences to be able to participate in the crystallization process. The decrease of the crystallinity and the melting point with increasing short chain branching content (part 1) can hence be explained by the thinner crystalline lamellar core thicknesses of the fractions. The results furthermore confirm previous results of Alamo et al.[27,36] and Hosoda et al.[10] that the lamellar thickness is determined by the ethylene sequence length between the branches and that the branches are preferentially rejected from the crystalline core, resulting in increased transition layer thicknesses.

The shape of the one-dimensional correlation function is also related to the arrangement of the lamellae in stacks. For an ideal lamellar system $\gamma_1(x)$ reaches a first positive maximum at a distance corresponding to the periodicity L. As can be seen in Figure 8, the maximum cannot be observed for fractions A6, A7, and A8. This lack of a clear maximum is induced by deviations from the ideal lamellar model. Broad thickness distributions of the crystalline or amorphous layers as well as the presence of nonparallel layers are resulting in such deviating lamellar stacks.[17,37] The TEM results reported in part 2 showed that fractions A6–A8 exhibit broader crystalline thickness distributions due to the decreasing branching content. Furthermore, the lamellae of these fractions have shorter lateral dimensions and a disturbed growth direction due to the increased molecular weight. Hence, for fractions A6–A8, both the branching content and the molar mass enhance the deviation from the ideal lamellar model.

Inspection of the data from the SAXS analysis as reported in Tables II and III and comparison with our TEM results on the same fractions allow us to check the validity of the two-phase and the pseudo-two-phase models. The average lamellar thickness C_l (two-phase model) exceeds the value $\langle T_c \rangle_n$ (pseudo-two-phase model), as the lamellar stacking deviates from the ideal model (fractions A6 and A7). The difference between the values of C_l and $\langle T_c \rangle_n$ clearly illustrates the need for a more reasonable model to account for the experimental facts. Although the two-phase model provides an easy and fast method for the calculation of the lamellar thickness, the assumed model is certainly unsatisfactory for the true lamellar morphology. For the fractions with an increased molecular weight, the entanglement effect causes a discontinuation of the growth direction of the lamellae, resulting in stacks of nonparallel lamellae. This fact is not accounted for in the simple two-phase concept. The correlation function approach, on the other hand, is valid for any pseudo-two-phase structure.[18,22] This was also the conclusion of Vonk,[38] who showed in a recent study of 31 polyethylene samples that the values of C_l are, on average, overestimated by as much as 42% as compared to those obtained with other models which take profit of the full information content of the scattering data. Analysis of the small-angle X-ray scattering intensity function always suffers from the difficulty that the significance of the data strongly depends on the validity of the proposed morphological model. Therefore, SAXS experiments should always be complemented with morphological information obtained with other techniques such as TEM.

Evaluation of the Results Obtained with TEM and SAXS. The lamellar thickness $\langle l_c \rangle$ as derived by TEM includes both the core and the transition layers, as was shown by Strobl et al.[19] As can be seen in Figure 9 the sum of the thickness of the core and the transition layers ($C + 2E$), as determined by SAXS, is in good agreement with the values obtained by TEM. The difference between the values obtained using two completely different techniques is not higher than 10 Å. This fair agreement probably results from the fact that the thickness distributions of the lamellae are relatively narrow. This is in

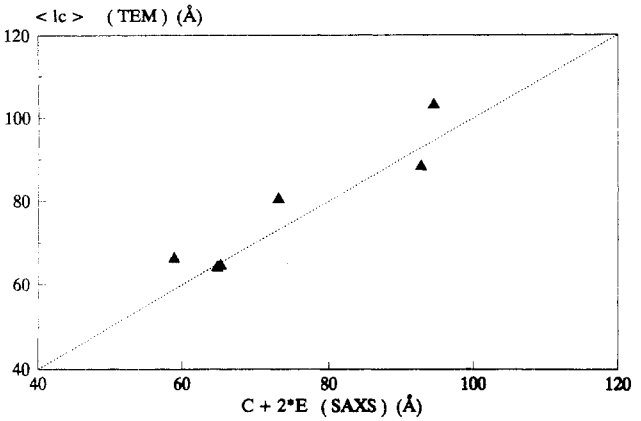

Figure 9. Sum of the thickness of the core and the transition layers ($C + 2E$) as determined by SAXS compared to values ($\langle l_c \rangle$) obtained by TEM.

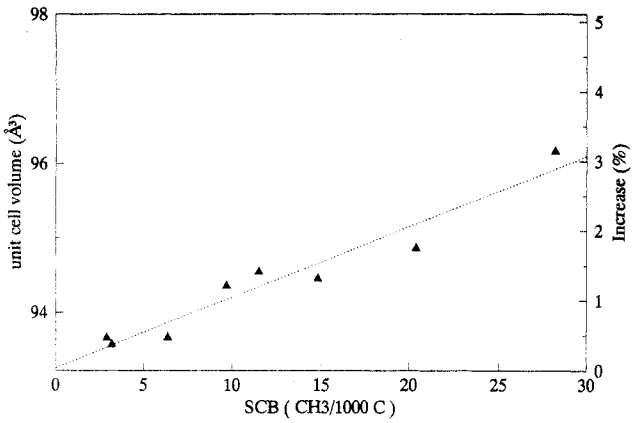

Figure 10. Unit cell volume as a function of the short chain branching content for fractions A2–A8 and the nonfractionated LLDPE A.

agreement with the conclusion of Voigt-Martin et al.,[24] who showed that there will be no correspondence between SAXS and TEM results when this condition is not fulfilled.

The TEM results revealed almost identical lamellar thickness distributions for samples A2–A4, despite their differences with respect to the short chain branching content. The lamellar thickness as measured with TEM includes however both the crystalline core and the transition layers. The present SAXS results now make clear that the increase of the transition layer thickness with increasing branching content obscures the further decrease of the crystalline core thickness, which could hence not be detected in the TEM study. This is further confirmed by the lowered crystallization and melting points of these fractions.[3]

Wide-Angle X-ray Scattering (WAXS)

Increasing the hexyl short chain branching content up to 30 CH_3/1000 C atoms results in a unit cell expansion of about 2% in the a direction and 1% in the b direction. The estimated standard deviation Δd was found to be 0.015 Å in the a direction and 0.010 Å in the b direction. For fractions A2 and A3, having the highest comonomer content, only three reflections—110, 200, and 210—were used since the other peaks could not be properly resolved; the estimated standard deviation is consequently higher and is about 0.070 Å in both directions. The unit cell volume shown in Figure 10 has been calculated assuming that the length of the unit cell in the molecular chain direction has a constant value[39] of 2.547 Å. The crystalline density ρ_c was calculated from the unit cell volume and

Table IV. Short Chain Branching Content, Unit Cell Parameters a and b, Unit Cell Volume, and Crystalline Density ρ_c of the Fractions and LLDPE A

sample	SCB (CH_3/1000 C)	a (Å)	b (Å)	V (Å^3)	ρ_c (g/cm^3)
A2	28.2	7.571	4.987	96.166	0.967
A3	20.4	7.500	4.966	94.863	0.980
A4	14.8	7.474	4.962	94.458	0.984
A5	11.5	7.469	4.970	94.547	0.983
A6	6.4	7.434	4.947	93.669	0.992
A7	3.2	7.422	4.950	93.574	0.993
A8	2.9	7.429	4.950	93.662	0.993
LLDPE A	9.7	7.468	4.961	94.363	0.985

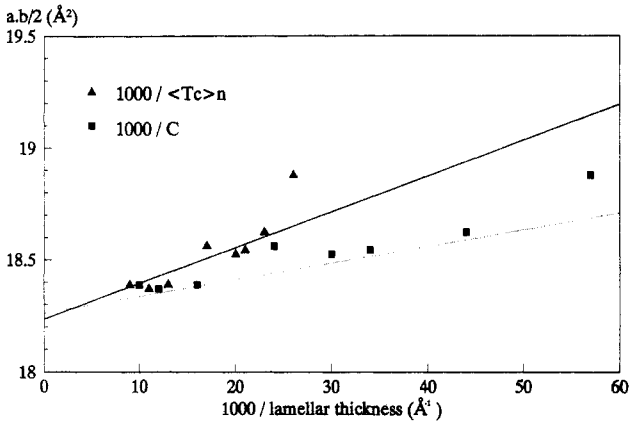

Figure 11. Chain cross-section ($ab/2$) vs the inverse lamellar thickness for fractions A2–A8 and LLDPE A: linear polyethylene (—); n-paraffins (···).

is presented together with the unit cell dimensions in Table IV. The measured values are in good agreement with results obtained for other copolymer samples.[39-43]

As was shown by Vand and de Boer[44] the unit cell volume of the n-paraffins depends on the thickness of the crystals that are formed. These authors predicted that the average cross-section of the unit cell normal to the chain direction would be related to the crystal thickness by relation 5, where p is a constant and C is the length of the paraffin chain.

$$\frac{ab}{2} = \left(\frac{ab}{2}\right)_0\left(1 + \frac{p}{C}\right) \tag{5}$$

This relation was later confirmed by Davis et al.[45] and extended to linear polyethylene crystallized from solution as well as from the melt. Vonk et al.[46] evaluated several HDPE and LLDPE samples and found in general a good correspondence with the relation established for n-paraffins. Increasing the molecular weight or the crystallization rate resulted in small positive deviations which could be explained by an increased entanglement density and stresses at the lamellar surface. For the 1-propene-based samples, however, larger deviations were observed. The authors tentatively interpreted these results by assuming that the methyl groups are incorporated in the lattice by interstitial solution.

In Figure 11 the chain cross-section ($ab/2$) of the different fractions and the LLDPE A sample is plotted versus the inverse average lamellar thickness ($1000/\langle T_c \rangle_n$) and is found to be in agreement with the relation found for melt-crystallized linear polyethylene.[45] The second set of data points in Figure 11 is constructed by plotting the chain cross-section versus the inverse average core thickness ($1000/C$), as determined with SAXS. For these data points, a good agreement is found with the relation for n-paraffins.[45] This observation illustrates that the transition layer—which has been accounted for in the first

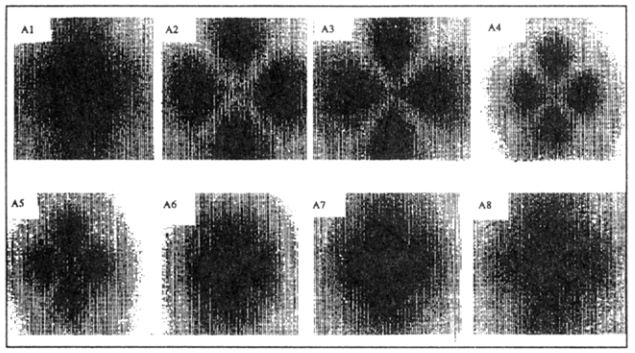

Figure 12. H_v SALLS scattering patterns of fractions A1–A8.

data set (▲), and not in the second one (■)—is indeed an important factor with respect to the understanding of the differences in the unit cell expansion of *n*-paraffins and linear polyethylene.

Small-Angle Laser Light Scattering (SALLS)

The H_v SALLS scattering patterns of the fractions recorded at room temperature after crystallization from the melt are shown in Figure 12. Fractions A2–A5, with high short chain branching content, are characterized by a clover-leaf light scattering pattern with fourfold symmetry and four lobes of high intensity.

Such scattering patterns are indicative for well-developed spherulitic morphologies.[47] With decreasing branching content (fractions A6–A8) the scattering patterns have a fourfold symmetry but the intensity at very low angles increases. This "tennis racket" type of scattering pattern points to an increasing degree of imperfection in the shape or in the internal structure of the spherulites as was shown by Mandelkern et al.[7] and Stein et al.[47] The higher weight-average molecular weight (from 176 300 to 269 000) of these fractions is undoubtedly at the basis of a less developed spherulitic morphology.[48] Fraction A1, having the highest comonomer content and a crystallinity of about 10%, has a scattering pattern with fourfold symmetry as well. The scattering intensity has a maximum in the center and decreases monotonically with increasing scattering angle, characteristic for rodlike aggregates of lamellae.[47]

The changes of the spherulitic morphology of the fractions as a function of the short chain branching content and the molar mass are in agreement with the morphological maps established for low-density polyethylene (LDPE) by Mandelkern[7,8] and for LLDPE by Hosoda.[10]

For the scattering patterns having well-defined lobes, the scattering angle θ_{max}, corresponding to the maximum intensity and consequently the average spherulitic radius, can be accurately determined. As can be seen in Figure 13, this results in the formation of spherulites with a smaller average radius when the short chain branching content is increased.

Conclusions

The morphology of narrowly branched fractions of a 1-octene LLDPE has been studied on the level of the semicrystalline lamellae, the unit cell, and the spherulitic morphology using several complementary techniques. The average short chain branching content of the eight fractions studied increases from 2.9 to 28.2 branches per 1000 carbon atoms, and the weight-average molecular weight decreases from 2.7×10^5 down to 1.9×10^4.

Detailed information on the lamellar morphology was obtained from SAXS experiments. The short chain branching content is the dominant characteristic of the chain microstructure with respect to the lamellar thickness.

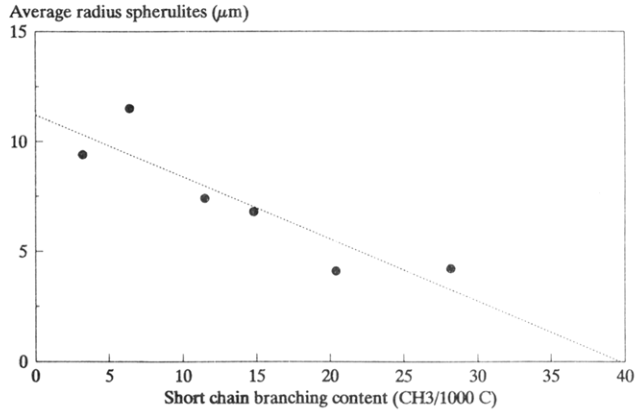

Figure 13. Average spherulitic radius as a function of the short chain branching content for fractions A2–A7.

Assuming a simple two-phase model for the lamellar morphology results in an overestimation of the lamellar thickness. Reliable results are obtained from the assumption of a pseudo-two-phase lamellar structure. A decrease of the crystalline core thickness C and an increase of the transition layer thickness E with increasing short chain branching content is observed. At the highest short chain branching content the transition layers are of the same order of magnitude as the core of the lamellae. Fair agreement was found between the thickness of the crystalline core and the transition layers ($C + 2E$) as obtained with SAXS and the values obtained in part 2 with TEM. The decrease of the melting point of the fractions shown in part 1 are also in agreement with the decrease of the core thickness C.

The unit cell expansion with increasing branching content is clearly related to the changes of the lamellar thickness. The chain folding process and the existence of a transition layer, where the side branches are accumulated, generate stresses at the lamellar surface, resulting in an increase of the chain cross-sectional area. With decreasing lamellar thickness the surface layers become relatively more important, and consequently the average unit cell is expanded. The overall chain microstructure (branching content and molecular weight) determines the spherulitic morphology as measured with SALLS. The average radius of the spherulites decreases with increasing short chain branching content. At high values of either the branching content or the weight-average molecular weight, well-developed spherulites are no longer observed.

Acknowledgment. H.R. is indebted to the Fonds voor Kollektief Fundamenteel Onderzoek, Belgium, and the Nationale Raad voor Wetenschappelijk Beleid (Synchro 9), Belgium, for financial support.

References and Notes

(1) Schouterden, P.; Groeninckx, G.; Van der Heijden, B.; Jansen, F. *Polymer* **1987**, *28*, 2099.
(2) Schouterden, P.; Vandermarliere, M.; Riekel, C.; Koch, M. H. J.; Groeninckx, G.; Reynaers, H. *Macromolecules* **1989**, *22*, 237.
(3) Defoor, F.; Groeninckx, G.; Schouterden, P.; Van der Heijden, B. *Polymer* **1992**, *33*, 3878.
(4) Defoor, F.; Groeninckx, G.; Schouterden, P.; Van der Heijden, B. *Polymer*, in press.
(5) Voigt-Martin, I. G.; Alamo, R.; Mandelkern, L. *J. Polym. Sci., Polym. Phys. Ed.* **1986**, *24*, 1283.
(6) Voigt-Martin, I. G.; Mandelkern, L. *Handbook of Polymer Science and Technology*; Cheremisinoff, N., Ed.; Dekker: New York, 1989; Vol. 3.
(7) Mandelkern, L.; Maxfield, J. *J. Polym. Sci., Polym. Phys. Ed.* **1979**, *17*, 1913.
(8) Mandelkern, L.; Glotin, M.; Benson, R. *Macromolecules* **1981**, *14*, 22.

(9) Voigt-Martin, I. G.; Mandelkern, L. *J. Polym. Sci., Polym. Phys. Ed.* **1981**, *19*, 1769.
(10) Hosoda, S.; Kojima, K.; Furuta, M. *Makromol. Chem.* **1986**, *187*, 1501.
(11) Stein, R. S.; Rhodes, M. B. *J. Appl. Phys.* **1960**, *31*, 1873.
(12) Stein, R. S.; Chu, W. *J. Polym. Sci., Part A-2* **1970**, *8*, 1137.
(13) Yoon, D. Y.; Stein, R. S. *J. Polym. Sci., Polym. Phys. Ed.* **1974**, *12*, 763.
(14) Brown, A.; Edmonds, J. W. *Adv. X-ray Anal.* **1980**, *23*, 361.
(15) Novak, G. A.; Colville, A. A. *Am. Mineral.* **1989**, *74*, 488.
(16) Defieuw, G. Ph.D. Thesis, K. U. Leuven, 1989.
(17) Vonk, C. G.; Kortleve, G. *Kolloid Z. Z. Polym.* **1967**, *220*, 19.
(18) Strobl, G. R.; Schneider, M. *J. Polym. Sci., Polym. Phys. Ed.* **1980** *18*, 1343.
(19) Strobl, G. R.; Schneider, M. J.; Voigt-Martin, I. G. *J. Polym. Sci., Polym. Phys. Ed.* **1980**, *18*, 1361.
(20) Vonk, C. G. *J. Appl. Crystallogr.* **1973**, *6*, 81.
(21) Crist, B. *J. Polym. Sci., Polym. Phys. Ed.* **1973**, *11*, 635.
(22) Vonk, C. G.; Pijpers, A. P. *J. Polym. Sci., Polym. Phys. Ed.* **1985**, *23*, 2517.
(23) Vonk, C. G. *J. Appl. Crystallogr.* **1975**, *8*, 340.
(24) Voigt-Martin, I. G.; Mandelkern, L. *J. Polym. Sci., Polym. Phys. Ed.* **1989**, *27*, 967.
(25) Braña, M. T. C.; Sainz, J. I. I.; Terselius, B.; Gedde, U. W. *Polymer* **1989**, *30*, 410.
(26) Wunderlich, B. In *Macromolecular Physics: Crystal Structure, Morphology and Defects*; Academic Press: New York, 1973; Vol. 1.
(27) Alamo, R.; Domszy, R.; Mandelkern, L. *J. Phys. Chem.* **1984**, *88*, 6587.
(28) Mathot, V. B. F.; Pijpers, M. F. J. *Polym. Bull.* **1984**, *11*, 297.
(29) Mandelkern, L.; Alamo, R. G.; Kennedy, M. A. *Macromolecules* **1990**, *23*, 4721.
(30) Voigt-Martin, I. G.; Mandelkern, L. *J. Polym. Sci., Polym. Phys. Ed.* **1984**, *22*, 1901.
(31) Hser, J. C.; Carr, S. H. *Polym. Eng. Sci.* **1979**, *19*, 436.
(32) Alamo, R. G.; Mandelkern, L. *Macromolecules* **1991**, *24*, 6480.
(33) Alamo, R. G.; Mandelkern, L. *Macromolecules* **1989**, *22*, 1273.
(34) Defoor, F. Ph.D. Thesis, K. U. Leuven, 1992.
(35) Randall, J. C.; Ruff, C. J. *Macromolecules* **1988**, *21*, 3446.
(36) Alamo, R. G.; Glaser, R. H.; Mandelkern, L. *J. Polym. Sci., Polym. Phys. Ed.* **1988**, *26*, 2169.
(37) Lee, Y. D.; Phillips, P. J.; Lin, J. S. *J. Polym. Sci., Polym. Phys. Ed.* **1991**, *29*, 1235.
(38) Vonk, C. G. *Makromol. Chem., Macromol. Symp.* **1988**, *15*, 215.
(39) Swan, P. R. *J. Polym. Sci.* **1962**, *56*, 409.
(40) Shirayama, K.; Kita, S.; Watabe, H. *Makromol. Chem.* **1972**, *151*, 97.
(41) Martinez de Salazar, J.; Baltá Calleja, F. J. *J. Cryst. Growth* **1980**, *48*, 283.
(42) Heink, M.; Häberle, K.-D.; Wilke, W. *Colloid Polym. Sci.* **1991**, *269*, 675.
(43) Howard, P. R.; Crist, B. *J. Polym. Sci., Polym. Phys. Ed.* **1989**, *27*, 2269.
(44) Vand, V.; de Boer, J. H. *Proc. K. Ned. Akad. Wet.* **1947**, *50*, 991.
(45) Davis, G. T.; Weeks, J. J.; Martin, G. M.; Eby, R. K. *J. Appl. Phys.* **1974**, *45*, 4175.
(46) Vonk, C. G.; Reynaers, H. *Polym. Commun.* **1990**, *31*, 192.
(47) Go, S.; Mandelkern, L.; Prud'homme, R.; Stein, R. S. *J. Polym. Sci., Polym. Phys. Ed.* **1974**, *12*, 1485.
(48) Bassett, D. C.; Hodge, A. M.; Olley, R. H. *Faraday Soc. Discuss.* **1979**, *68*, 218.